The Impact of Ground Heat Capacity on Drinking Water Temperature

Sarai Díaz[1], Joby Boxall[2], Louis Lamarche[3], and Javier González[4]

[1]Corresponding author: Dr. Eng, Deptartment of Civil Engineering, University of Castilla-La Mancha, Av. Camilo José Cela s/n, 13071 Ciudad Real (Spain). E-mail: Sarai.Diaz@uclm.es

[2]Dr. Eng, Penine Water Group, Department of Civil and Structural Engineering, The University of Sheffield, S1 3JD, Sheffield, United Kingdom. E-mail: j.b.boxall@sheffield.ac.uk

[3]Dr. Eng, École de Technologie Supérieure, 1100 Notre-Dam Street West, H3C 1K3, Montreal, Canada. E-mail: Louis.Lamarche@etsmtl.ca

[4]Dr. Eng, Deptartment of Civil Engineering, University of Castilla-La Mancha, Av. Camilo José Cela s/n, 13071 Ciudad Real (Spain). // HIDRALAB INGENIERÍA Y DESARROLLOS, S.L., Spin-Off UCLM, Hydraulics Laboratory Univ. of Castilla-La Mancha, Av. Pedriza, Camino Moledores s/n, 13071 Ciudad Real (Spain). E-mail: Javier.Gonzalez@uclm.es

The final published version is available at
https://ascelibrary.org/doi/10.1061/JWRMD5/WRENG-5869

ABSTRACT

Temperature is known to impact physical, chemical and biological processes in Drinking Water Distribution Systems (DWDS), but it is rarely considered or modelled. This research evaluates the impact of considering a finite heat capacity for the ground, which has been assumed infinite in previous DWDS research. The aim of this work is to explore and quantify the region where the difference between considering infinite or finite heat capacity for the ground is significant, i.e. the distance over which water-ground heat transfer interaction is important. A detailed model comparison is carried out for key pipe materials, diameters and hydraulic conditions. Temperature

effects are found to exist for up to tens of kilometres (i.e. several hours) into the DWDS. While the differences found were only a few degrees Celsius, this will affect all reaction rates, such as chlorine decay, and is at the start of the DWDS so will impact the entire downstream network. This work highlights the importance of considering temperature in DWDS, and in particular the finite heat capacity of the ground, in ensuring the provision of safe drinking water.

INTRODUCTION

Temperature affects all physical, chemical and biological processes occurring within Drinking Water Distribution Systems (DWDS). In general, temperature increase is associated with water quality deterioration. For example, it is well-known that temperature increases the rate at which chlorine decays (Fisher et al. 2012; Monteiro et al. 2017). This is important for the operation of DWDS, as many countries aim to ensure a minimum target level of disinfectant at the customer tap to minimise risks to public health (WHO 2011). Temperature is also known to affect bacterial-fungal communities (Calero et al. 2021) and precipitation reactions like iron and manganese (Mounce et al. 2016), potentially contributing to discolouration. At present, there is hardly any temperature monitoring, so it is not easy to see trends and/or quantify the implications of temperature increase on water quality (Agudelo-Vera et al. 2020). The data that is available shows that there is correlation with water quality and air temperature, e.g. higher discolouration contacts during summer (van Summeren et al. 2015; Cook et al. 2015). This justifies the current need to monitor and better understand temperature dynamics within DWDS, especially in the face of climate change challenges.

Hydraulic and water quality models usually consider a constant temperature (Fisher et al. 2012). According to Agudelo-Vera et al. (2020), only Blokker and Pieterse-Quirijns (2013) and Piller and Tavard (2014) present validated models to compute water temperature across DWDS. Both rely on assuming a fixed ground temperature that constitutes the boundary condition for heat transfer to the fluid. This is equivalent to assume an infinite heat capacity for the ground, which remains unaffected by heat exchange to and from the water within the pipes. This simplification enables a decoupling of the problem: (1) calculate the undisturbed ground temperature, and (2) calculate the water temperature based on the previously estimated ground temperature (typically a daily

average). Blokker and Pieterse-Quirijns (2013) propose a micrometeorology model to compute the undisturbed ground temperature and then use EPANET-MSX (Shang et al. 2008) to simulate water temperatures. After analysing several Dutch case studies, they conclude that water reaches the ground temperature at a rate that depends on pipe diameter, pipe thickness, pipe material and flow velocity. This simplified heat transfer model enables identification of overall water temperature behaviours: water temperature in transport mains stays similar to that at the inlet, whereas water temperature in distribution mains approaches the undisturbed ground temperature. What happens in between, i.e. how large and significant is the transition zone, has not been specifically addressed. To compute this region, it is important to acknowledge that in reality ground has a finite heat capacity and the temperature of the ground around a pipe is affected by the drinking water temperature (and vice versa), i.e. it is a coupled problem. In winter, input water is usually colder than the ground, so water heats over the pipeline and the surrounding ground loses temperature in the process. In summer, incoming water is likely to be warmer than the ground, so water cools along the pipeline and the surrounding ground heats in the process. Even though the few studies that address temperature modelling at DWDS usually make the infinite ground heat capacity hypothesis (Blokker and Pieterse-Quirijns 2013; Piller and Tavard 2014), it is known that the heat transfer process is a complex phenomenon (Agudelo-Vera et al. 2020).

The importance of fluid-ground interaction has been studied for other buried pipe infrastructure systems where the temperature difference between the ground and the fluid is larger and so it is not acceptable to assume infinite heat capacity for the ground. This is the case of sewer systems, where temperature modelling has become important to assess the potential of heat recovery applications. In these systems, it is usual to assume a penetration depth for heat exchange around the sewer. The ground temperature is usually measured, and the depth of this influence area (where heat conduction through the ground takes place) is usually adjusted (Durrenmatt and Wanner 2008; Abdel-Aal et al. 2014). This approach is effectively approximately equivalent to considering a finite heat capacity for the ground within a zone of influence. It is highly dependent on field measurements, so its application is empirical, relying on physically measured temperature data

from the ground around pipes. Ground-fluid temperature interaction has also been studied in the context of Ground Source Heat Pumps (GSHP). These systems are specifically designed to exploit the temperature difference between the circulating fluid and the ground for different purposes (Soni et al. 2015). For these applications it is essential to consider the finite heat capacity of the ground to correctly model thermal interaction. Horizontal GSHP extend beneath the ground surface in a similar way to DWDS. Their behaviour can be modelled experimentally, numerically or analytically (Gan 2019). Analytical approaches are especially interesting because they have potential to provide a conceptual framework for systematic assessment. Most analytical approaches compute fluid temperature variation along the pipe according to the Finite Line Source (FLS) model: the pipe behaves as a line that releases or receives heat within a semi-infinite ground domain (Claesson and Dunand 1983; Fontaine et al. 2011). GSHP have a well-established steady analysis. Unsteady analysis involves a temporal convolution that is time-consuming to solve (Lamarche 2017). Several researchers have proposed the use of accelerating schemes to solve this convolution, like the Fast Fourier Algorithm (Marcotte and Pasquier 2008). Such an approach requires knowledge of the heat history beforehand, which is not trivial in systems that run near the ground surface (both horizontal GSHP and DWDS), because they are exposed to weather variations (Lamarche 2017). Lamarche (2019) has recently proposed a non-history scheme to compute the heat transfer and output fluid temperature based on the input fluid temperature evolution over time. This unsteady ground model could be applied at DWDS to assess the impact of water-ground heat transfer interaction at different periods of the year.

The main objective of this paper is to assess the importance of ground heat capacity on drinking water temperature. This is possible by fulfilling three specific aims. First, to compare the water temperatures obtained with the usually adopted decoupled model (infinite ground heat capacity) and a more realistic coupled approach (finite ground heat capacity). The importance of making one assumption or the other can be assessed by estimating the transition region. The transition region is here defined as the distance or equivalent residence time required for the water to attain the undisturbed ground temperature. It represents the region where heat interaction is important.

Therefore, the second aim of this work is to quantify the transition region. We aim to derive an explicit expression to compute the transition region by assuming steady flow and ground conditions, but requiring simplification of the less tractable unsteady ground behaviour. Thus, the third aim of this paper is to assess if the analytical expression derived when considering steady ground conditions can approximate transition regions when considering the annual cycle of the ground and input water temperatures. The novelty of this work lies in providing a conceptual framework to better describe the steady and unsteady water-ground heat transfer interaction of DWDS. Our hypothesis is that there is a significant transition region and hence that assuming infinite ground heat capacity is not a good enough approximation for a significant part of the DWDS.

METHODOLOGY

The steady and unsteady approaches presented in this section build on the principles of ground heat transfer. Note that steady flow conditions will be assumed as a first approximation to the complex heat interaction problem.

2.1 Ground heat transfer principles

Figure 1 shows a pipe buried in the ground and exchanging heat between the ground and the fluid that is being transported. Assuming that the ground is a homogeneous semi-infinite medium, its temperature distribution $T(t, x, y, z)$ behaves according to the heat conduction equation (Lamarche 2019):

$$\frac{1}{\alpha_{ground}} \frac{\partial T(x, y, z, t)}{\partial t} = \nabla^2 T(x, y, z, t) \tag{1}$$

with

$$T(x, y, 0, t) = T_{surf}(t) \tag{2}$$

$$q''(t) = -k_{ground} \frac{\partial T(x, y, z, t)}{\partial n}\Big|_{r=r_p} \tag{3}$$

Note that T represents the temperature field in the ground and $\alpha_{ground}[m^2/s] = \frac{k_{ground}}{\rho_{ground} \cdot C_{ground}}$ is the thermal diffusivity of the ground, which can be obtained by dividing its conductivity $k_{ground}[W/m/K]$ by its density $\rho_{ground}[kg/m^3]$ and specific heat capacity $C_{ground}[J/kg/K]$.

Eq. (2) represents the boundary condition at the surface $T_{surf}(t)$ and Eq. (3) the heat exchange with the pipe, where $q''[W/m^2]$ is the heat flux per unit area and $r_p[m]$ the pipe radius (radial coordinates).

Due to the linearity of the heat equation, the solution to the problem is typically computed by making use of the superposition principle (Claesson and Dunand 1983). According to this principle, the original problem can be divided in two (see Figure 1): (1) computing the temperature field associated with the heat extraction/release to the pipe, assuming that there is a zero-temperature boundary condition at the ground surface, and (2) computing the temperature field associated with the changing surface temperature, as if there was no pipe:

$$T(x, y, z, t) = {}^1T(x, y, z, t) + {}^2T(z, t) \tag{4}$$

Note that problem 2 aims to compute the temperature field of the undisturbed ground at a depth z, disregarding the presence of the pipe. Therefore, it can be solved by assuming a surface temperature behaviour $T_{surf}(t)$, which propagates through the ground. Different models can be adopted to simulate the surface temperature. For example, it can be modelled by assuming an annual sinusoidal variation at the ground boundary (Lamarche 2019):

$$T_{surf}(t) = T_0 - A \cdot \cos(\omega \cdot (t - t_{shift})) \tag{5}$$

Kusuda and Achenbach (1965) proposed an analytical solution for this boundary condition:

$${}^2T(z, t) = T_0 - A \cdot \exp\left(-z\sqrt{\frac{\omega}{2 \cdot \alpha_{ground}}}\right) \cdot \cos\left(\omega \cdot (t - t_{shift}) - z\sqrt{\frac{\omega}{2 \cdot \alpha_{ground}}}\right) \tag{6}$$

Where $T_0[°\mathrm{C}]$ is the mean ground surface temperature, $A[°\mathrm{C}]$ is the variation amplitude of temperature at the surface , $\omega = 2\pi/8760\ h^{-1}$ is the annual frequency, $t_{shift}[h]$ is the time for the coldest day of the year and $\alpha_{ground}[m^2/h]$ is the thermal diffusivity of the ground. Thermal diffusivity is here expressed in m^2/h to be consistent with annual simulations, which are typically carried out

every hour when analysing ground temperatures (Lamarche 2019). Thermal diffusivity is a critical parameter when computing the undisturbed ground temperature distribution and is here assumed constant over the simulation period. Sand is typically used as backfill for pipe installation. Table 1 shows typical ground parameters for an average dry and wet sand (Blokker and Pieterse-Quirijns 2013). Figure 2 shows the corresponding temperature distributions over a year according to Eq. (6) at different depths. More complex models exist and could be used to simulate the undisturbed ground temperature, leading to different shapes in Figure 2, but they will not impact the core of the questions that this paper aims to answer. Note that pipes are usually buried at depths between 0.6-2.5 m depending on the country (Agudelo-Vera et al. 2020). Blokker and Pieterse-Quirijns (2013) observed that there is a damping effect of air temperature daily variations at a 1 m depth in a case study in The Netherlands. This supports the assumption of only considering annual variations for the ground temperature at usual pipe depths.

2.2 Steady ground model

Section 2.1 has shown that the ground experiences annual changes over the year. However, a simplified steady state approach can be assumed to start simulating the heat exchange when considering periods of days or weeks. The fluid temperature and heat variation along a horizontal pipe has been studied before for the steady-state case (Claesson and Dunand 1983). Fluid temperature decays exponentially along the pipe (Fontaine et al. 2011), so the water temperature when considering a ground surface temperature equal to 0ºC (problem 1 in Figure 1) would be equal to:

$$T_w(x) = T_{in} \cdot \exp\left(\frac{-x}{Q \cdot \rho_w \cdot C_w \cdot R}\right) \tag{7}$$

Where $T_w(x)[^\circ\mathrm{C}]$ represents the water temperature at a distance x from the inlet, $T_{in}[^\circ\mathrm{C}] = T_w(0)$ represents the water temperature at the inlet, $Q[m^3/s]$ is the water volume flow rate, $\rho_w[kg/m^3]$ is the fluid density, $C_w[J/kg/K]$ is the water specific heat capacity and $R[m \cdot K/W]$ is the unit length thermal resistance. Eq. (7) can be referenced to the undisturbed ground temperature (problem 2 in

Figure 1) by applying superposition:

$$T_w(x) = (T_{in} - T_{ground}) \cdot \exp\left(\frac{-x}{Q \cdot \rho_w \cdot C_w \cdot R}\right) + T_{ground} \tag{8}$$

Where $T_{ground}[°\text{C}] = {}^2T(z_p, \infty)$ represents the undisturbed ground temperature at the installation pipe depth z_p in an infinite time (i.e. steady state). Note that the installation depth is here assumed equal to the difference in elevation between the ground surface and the center line of the pipe. This is a simplification required for the analytical steady approach to be consistent with the unsteady ground model presented in Section 2.3. Figure 2 shows the undisturbed ground temperature evolution at the center line of a 300 mm diameter pipe buried at $z_p = 1$ m, as well as at its top ($z = 0.85$ m) and bottom ($z = 1.15$ m). The maximum difference is approximately 1ºC, i.e. there are $\pm 0.5°C$ deviations with respect to the temperature at the center of the pipe through the year. At the same time, the installation depth refers to the elevation of the center line of the pipe in the middle of the pipeline.

Thermal resistance can be computed as a summation of resistances (Çengel and Ghajar 2011), which is different depending on whether the heat transfer interaction is considered or not:

$$R = \frac{\ln(\frac{2 \cdot z_p}{r_o})}{2 \cdot \pi \cdot k_{ground}} + \left(\frac{\ln(\frac{r_o}{r_i})}{2 \cdot \pi \cdot k_{pipe}} + \frac{1}{Nu \cdot k_w \cdot \pi}\right) = R_{ground} + R_{pipe} \tag{9a}$$

$$R = \left(\frac{\ln(\frac{r_o}{r_i})}{2 \cdot \pi \cdot k_{pipe}} + \frac{1}{Nu \cdot k_w \cdot \pi}\right) = R_{pipe} \tag{9b}$$

Where $r_o[m]$ and $r_i[m]$ represent the inner and outer pipe radius, $k_{pipe}[W/m/K]$ is the pipe conductivity, $k_w[W/m/K]$ is the water conductivity and $Nu[-]$ is the Nusselt number, which must be computed as:

$$Nu = \begin{cases} 3.66 & \text{if } Re < 2300 \\ \frac{(f/8) \cdot (Re - 1000) \cdot Pr}{1 + 12.7 \cdot (f/8)^{0.5} \cdot (Pr^{\frac{2}{3}} - 1)} & \text{if } Re \geq 2300 \end{cases} \tag{10}$$

where $f[-]$ represents the friction factor, $Re[-]$ is the Reynolds number and $Pr[-]$ corresponds

to the Prandtl number:

$$Re = \frac{\rho_w \cdot v \cdot 2 \cdot r_i}{\mu_w} \tag{11}$$

$$Pr = \frac{\mu_w \cdot C_w}{k_w} \tag{12}$$

with $v[m/s]$ being equal to the water velocity and $\mu_w[kg/m/s]$ representing the dynamic viscosity of water.

Note that Eq. (9a) includes three terms that correspond to heat conduction through the ground, heat conduction through the pipe wall and convection through water, respectively. In other words, the first term is related to the ground $R_{ground}[m \cdot K/W]$ (Claesson and Dunand 1983; Fontaine et al. 2011; Lamarche 2019) and the other two (within brackets) refer to the pipe $R_{pipe}[m \cdot K/W]$. All terms should be considered when analysing the water-ground interaction (i.e. Eq. 9a to simulate the ground finite heat capacity), but only the last two terms (R_{pipe}) should be considered when disregarding this interaction (i.e. Eq. 9b to assume an infinite heat capacity for the ground). The implications of assuming Eq. (9a) or (9b) will be discussed in Section 3.1, where Eqs. (8) and (9) will be applied to assess the temperature evolution over a pipeline under steady state conditions.

Eqs. (8) and (9) can be rearranged to explicitly compute the transition length ($L_t[m]$). This length is quantified by identifying the position where the absolute error between the undisturbed ground temperature and the water temperature is lower than a specified tolerance, i.e. $|T_w - T_{ground}| \leq tol$. This leads to:

$$\begin{aligned} L_t &= Q \cdot \rho_w \cdot C_w \cdot [R_{ground} + R_{pipe}] \cdot \ln\left(\frac{|T_{in} - T_{ground}|}{tol}\right) = \\ &= Q \cdot \rho_w \cdot C_w \cdot \left[\frac{\ln(\frac{2 \cdot z_p}{r_o})}{2 \cdot \pi \cdot k_{ground}} + \left(\frac{\ln(\frac{r_o}{r_i})}{2 \cdot \pi \cdot k_{pipe}} + \frac{1}{Nu \cdot k_w \cdot \pi}\right)\right] \cdot \ln\left(\frac{|T_{in} - T_{ground}|}{tol}\right) \end{aligned} \tag{13a}$$

$$\begin{aligned} L_t &= Q \cdot \rho_w \cdot C_w \cdot [R_{pipe}] \cdot \ln\left(\frac{|T_{in} - T_{ground}|}{tol}\right) = \\ &= Q \cdot \rho_w \cdot C_w \cdot \left[\left(\frac{\ln(\frac{r_o}{r_i})}{2 \cdot \pi \cdot k_{pipe}} + \frac{1}{Nu \cdot k_w \cdot \pi}\right)\right] \cdot \ln\left(\frac{|T_{in} - T_{ground}|}{tol}\right) \end{aligned} \tag{13b}$$

These transition lengths could be turned into equivalent residence times as L_t/v, where $v[m/s]$ is

the water velocity assuming average constant velocity. Note that Eq. (13a) provides the transition length when considering finite heat capacity for the ground (i.e. coupled model) and Eq. (13b) provides the equivalent assuming infinite heat capacity for the ground (i.e. decoupled model). As explained in the Introduction, assuming infinite heat capacity is the assumption made in the few existing applications for temperature modelling in DWDS and as has been coded to simulate network behaviour taking advantage of the EPANET-MSX functionality. Reality is coupled, and the difference between results obtained with Eqs. (13a) and (13b) will show the implications of simplifying by assuming infinite heat capacity.

2.3 Unsteady ground model

Section 2.1 has highlighted that seasonal changes in air temperature penetrate to typical DWDS pipe burial depths. Input water temperatures are also expected to change over the year according to temperature trends at the source water, water treatment plant and/or service reservoir. These annual changes will impact water temperature dynamics, and so the associated water quality.

The application of the ground model proposed by Lamarche (2019) to DWDS considers that the volume flow rate of the fluid $Q[m^3/s]$, the input water temperature record $T_{in}(t)[°\mathrm{C}]$ and the undisturbed ground temperature distribution ${}^2T(z,t)[°\mathrm{C}]$ determine the total heat transfer flux at each time $q(t)[W]$. They all condition the temperature at the end of the pipeline $T_{out}(t)[°\mathrm{C}]$ and the temperature of the ground at the pipe surroundings $T_p(t)[°\mathrm{C}]$. In this work, the formulation is explained for a prototypical water pipeline with a length $L[m]$ located at a constant depth $z = z_p[m]$ (horizontal pipe). Heat transfer flux cannot be assumed constant along the pipe due to the temporal and spatial variations in temperature gradients, so it is split into $n_s = L/L_i$ segments as proposed by Fontaine et al. (2011), where $L_i[m]$ is the length of each segment i. Therefore, the unknowns to be solved at each time step are the input water temperature at each segment except the first one $(T_{in,i}(t)[°\mathrm{C}]; \forall i = 2, \ldots, n_s)$ and the temperature of the ground at the surroundings of each pipe segment $(T_{p,i}[°\mathrm{C}]; \forall i = 1, \ldots, n_s)$.

The solution depends on how the temperature reduction $\theta_i[-]$ varies along each segment. It is

defined as:

$$\theta_i = \frac{\tilde{T}_{out,i}(t) - {}^1T_{p,i}(t)}{\tilde{T}_{in,i}(t) - {}^1T_{p,i}(t)} \tag{14}$$

with $\tilde{T}_{out,i}(t) = T_{out,i}(t) - {}^2T(z_p, t)$ and $\tilde{T}_{in,i}(t) = T_{in,i}(t) - {}^2T(z_p, t)$ according to the superposition principle and ${}^2T(z_p, t)$ given by Eq. (6). At the same time, temperature variation across each segment can be assumed to follow an exponential decay (Lamarche 2019):

$$\theta_i = \exp\left(\frac{-L_i}{Q \cdot \rho_w \cdot C_w \cdot R_{pipe}}\right) \tag{15}$$

Only $R_{pipe}\,[m \cdot K/W]$ is here considered as thermal resistance because the ground effect is considered in the unsteady ground model formulation. The pipe and the ground domains are later solved jointly through a system of equations (Eqs. 17 to 28). Note that assuming an exponential decay for each segment (Eq. 15) implies considering that water achieves the steady state at each time, neglecting the plug flow along the pipeline. This is a simplification (see Section 4), but it enables computation of an equivalent heat transfer coefficient $X_i\,[W/m/K]$ for each segment as:

$$X_i = \frac{Q \cdot \rho_w \cdot C_w}{L_i} \cdot (1 - \theta_i) \tag{16}$$

According to Lamarche (2019), the temperature in the pipe surroundings can be computed by considering the pipe segment interaction along the pipe:

$${}^1T_{p,i}(t) = S_{p,i}(t) + \sum_{j=1}^{n_s} S_{q,ij} \cdot X_j \cdot (\tilde{T}_{in,j}(t) - {}^1T_{p,j}(t)) \tag{17}$$

Where $S_{p,i}(t)$ and $S_{q,ij}$ illustrate the pipe segment interaction as a result of heat conduction through the ground (see Eqs. 31 to 36 below). As the temperature at the beginning of each segment must be equal to the temperature at the end of the previous segment (n_s in series pipes), Eq. (14) can be rewritten as an additional condition:

$$\tilde{T}_{in,i+1}(t) = \tilde{T}_{out,i}(t) = \theta_i \cdot \tilde{T}_{in,i}(t) + (1 - \theta_i) \cdot {}^1T_{p,i}(t) \tag{18}$$

Eqs. (17) and (18) can be rearranged as a system of equations where the coefficient matrix $\mathbf{A}$ remains constant and the independent term $\mathbf{B}(t)$ and unknown vector $\mathbf{T}(t)$ change over time:

$$\mathbf{A} \times \mathbf{T}(t) = \mathbf{B}(t) \tag{19}$$

The coefficient matrix can be built as:

$$\mathbf{A} = \begin{bmatrix} \mathbf{UL}(n_s \times n_s) & \mathbf{UR}(n_s \times n_a) \\ \mathbf{LL}(n_a \times n_s) & \mathbf{LR}(n_a \times n_a) \end{bmatrix} \tag{20}$$

With $n_a = n_s - 1$ and:

$$\mathbf{UL} = \begin{bmatrix} 1 + X_1 \cdot S_{q,11} & X_2 \cdot S_{q,12} & \cdots \\ X_1 \cdot S_{q,21} & 1 + X_2 \cdot S_{q,22} & \cdots \\ \vdots & \vdots & \ddots \end{bmatrix} \tag{21}$$

$$\mathbf{UR} = \begin{bmatrix} -X_2 \cdot S_{q,12} & -X_3 \cdot S_{q,13} & \cdots \\ -X_2 \cdot S_{q,22} & -X_3 \cdot S_{q,23} & \cdots \\ \vdots & \vdots & \ddots \end{bmatrix} \tag{22}$$

$$\mathbf{LL} = \begin{bmatrix} -(1 - \theta_1) & 0 & \cdots \\ 0 & -(1 - \theta_2) & \cdots \\ \vdots & \vdots & \ddots \end{bmatrix} \tag{23}$$

$$\mathbf{LR} = \begin{bmatrix} 1 & 0 & \cdots \\ -\theta_2 & 1 & \cdots \\ \vdots & \vdots & \ddots \end{bmatrix} \tag{24}$$

The independent term can be estimated as:

$$\mathbf{B}(t) = \begin{bmatrix} \mathbf{BU}(t)(n_s \times 1) \\ \mathbf{BL}(t)(n_a \times 1) \end{bmatrix} \tag{25}$$

With:

$$\mathbf{BU}(t) = \begin{bmatrix} S_{p,1}(t) + X_1 \cdot S_{q,11} \cdot \tilde{T}_{in,1}(t) \\ S_{p,2}(t) + X_1 \cdot S_{q,21} \cdot \tilde{T}_{in,1}(t) \\ \vdots \end{bmatrix} \tag{26}$$

$$\mathbf{BL}(t) = \begin{bmatrix} \tilde{T}_{in,1}(t) \cdot \theta_1 \\ 0 \\ \vdots \end{bmatrix} \tag{27}$$

The vector of unknowns would be:

$$\mathbf{T}(t) = \begin{bmatrix} {}^1\mathbf{T_p}(t)(n_s \times 1) \\ \tilde{\mathbf{T}}_{\mathbf{in}}(t)(n_a \times 1) \end{bmatrix} \tag{28}$$

Note that if the pipe has a different depth at the beginning and the end, the difference should be included in Eq. (27) as suggested by Lamarche (2019).

Once the system of equations in Eq. (19) is solved at a time t, ${}^1T_{p,i}(t)$ and $\tilde{T}_{in,i}(t)$ are known. The temperature at the end of each segment $\tilde{T}_{out,i}(t)$ can be directly computed according to Eq. (18). The heat flux per unit length at the next time step $q'_i(t + \Delta t)[W/m]$ can be computed as:

$$q'_i(t + \Delta t) = X_i \cdot \left(\tilde{T}_{in,i}(t) - {}^1T_{p,i}(t) \right) \tag{29}$$

so the total heat load $q(t + \Delta t)[W]$ can be obtained as:

$$q(t + \Delta t) = \sum_{i=1}^{n_s} q'_i(t + \Delta t) \cdot L_i \tag{30}$$

The process must then be repeated at the next time step. Solving these equations for the whole year would provide the annual water temperature evolution along the pipe. These values could be used to compute the transition length at any time.

Note that the only terms that have not been explained yet are $S_{p,i}(t)$ and $S_{q,ij}$. According to

Lamarche (2017) and Lamarche (2019), $S_{q,ij}$ can be computed as:

$$S_{q,ij} = \frac{1}{k_{ground}} \sum_{n=1}^{n_d} \left(1 - \exp(-d_n^2 \cdot \Delta\tilde{t})\right) \cdot u_{ij}(d_n) \cdot \Delta d_n \tag{31}$$

Where d_n is a dummy variable ($n_d = 450$ in this work), $\Delta\tilde{t} = \frac{\alpha_{ground} \cdot \Delta t}{r_o^2}$ is a dimensionless time interval and $u_{ij}(d)$ involves the inverse Laplace transform of the so-called g-function:

$$u_{ij}(d) = -\frac{d}{\pi} \cdot \mathbf{L}^{-1}(g_{ij}(t_k)) \tag{32}$$

The g-function is characteristic of the system. It was tabulated by Eskilson (1987) for different borehole (here equivalent to pipe) configurations, although several authors have worked on deriving analytical formulations (Zeng et al. 2003; Lamarche and Beauchamp 2007). Note that the g-function has been here expressed as a function of t_k because the Gavesh algorithm (Stehfest 1970; Villinger 1985) used to compute the associated Laplace transform needs to evaluate the function at some unknown times:

$$g_{ij}(t_k) = \frac{1}{2} \int_{\frac{1}{2\sqrt{\alpha_{ground} \cdot t_k}}}^{\infty} \frac{\exp(-r^2 \cdot s^2) - \exp(-r_{imag}^2 \cdot s^2)}{s^2} \cdot \{ierf[(\Delta x + L_j) \cdot s] - ierf[\Delta x \cdot s] + ierf[(\Delta x - L_i) \cdot s] - ierf[(\Delta x + L_j - L_i) \cdot s]\} \cdot ds \tag{33}$$

Where Δx refers to the difference between the initial coordinates of segment i and segment j ($\Delta x = x_{0,i} - x_{0,j}$), $r = r_o$, $r_{imag} = 2 \cdot z_p$, and the $ierf$ function is:

$$ierf(a) = a \cdot erf(a) - \frac{1}{\sqrt{\pi}} \cdot (1 - \exp(-a^2)) \tag{34}$$

On the other hand, $S_{p,i}(t)$ can be calculated as:

$$S_{p,i}(t) = \frac{1}{k_{ground}} \sum_{n=1}^{n_d} \exp(-d_n^2 \cdot \Delta\tilde{t}) \cdot F_i(\tilde{t}, d_n) \cdot \Delta d_n \tag{35}$$

316 Where $F_i(0, d_n) = 0$ and:

317 $$F_i(\tilde{t} + \Delta\tilde{t}, d_n) = \exp(-d_n^2 \cdot \Delta\tilde{t}) \cdot F_i(\tilde{t}, d_n) + \sum_{j=1}^{n_s} q'_j(\tilde{t} + \Delta\tilde{t}) \cdot (1 - \exp(-d_n^2 \cdot \Delta\tilde{t})) \cdot u_{ij}(d_n) \quad (36)$$

318 ## RESULTS

319 In this section, both the steady and the unsteady ground models will be applied to a case study.
320 It is important to highlight that both models have been presented assuming that steady flow (i.e.
321 constant volume flow rate) takes place within the pipe. This implies that the formulations here
322 proposed can only be applied where the flow can be approximated to steady state (i.e. assuming
323 approximation to average daily flow), while the ground surface and the input water temperatures
324 may experience changes according to the annual cycle. This simplification is reasonable when
325 seasonal effects are of interest and daily flows and/or temperature variations are not significant. In
326 this work, an average pipe located early in the DWDS will be analysed, as the temperature gradient
327 and so the effect of temperature exchange is greatest along the first kilometres (with how many
328 kilometres, or how much time, effects are important for a key unknown to be elucidated here).
329 Rather than trying to consider the unnecessary complexity of a real network, and in order to prevent
330 results from being arguably specific to the assumed layout, a single long pipe is considered to
331 enable generic estimation of the transition region in terms of distance and/or time.

332 This pipe is assumed to have a constant velocity $v = 0.5$ m/s and an internal radius $r_i = 0.15$
333 m (volume flow rate $Q = 0.0353 m^3/s$), which can be considered representative of the usual pipes
334 located early in a DWDS. The pipe is considered to be installed at a constant $z_p = 1$ m, which
335 is consistent with typical installation depths (Agudelo-Vera et al. 2020). As previously explained,
336 such a depth already implies that daily temperature oscillations are not perceived in the ground
337 (Blokker and Pieterse-Quirijns 2013). The pipe is considered to be extremely long, with $L = 125$
338 km, so that the simulated residence times are also high (69.4 h, almost 3 days). Note that the
339 average residence time in water systems at distribution level is 24 hours (Husband et al. 2008), and
340 even greater residence times might be obtained at some points (Machell and Boxall 2012; Machell

and Boxall 2014). Therefore, even though the case study is a large diameter pipe with steady flow, it will provide residence times that are representative of what could happen within the distribution level (see Section 4 for discussion). This length is associated with significant pressure drops along the pipeline. In real systems, different diameters and velocities exist along the pipeline, leading to more realistic pressure distributions.

Different materials will be considered, including unlined Cast Iron (CI), Asbestos Cement / Concrete (AC/C), PolyEthylene (PE) and PolyVinil Chloride (PVC). Table 2 summarises the prototypical characteristics assumed for these materials according to previous literature references (Blokker and Pieterse-Quirijns 2013; Blokker et al. 2014) and industry standards (Canal de Isabel II 2021). Pipe thickness $t_{pipe}[m]$ is here computed based on the assumed Standard Dimensional Ratio (SDR), which is considered characteristic of each material:

$$t_{pipe} = \frac{2 \cdot r_i}{SDR - 2} \tag{37}$$

In reality, SDR may change with the diameter and/or the age of the pipe (due to manufacturing evolution), but since the aim of this work is to analyse general behaviours and trends, assuming a constant value is considered sufficient.

In order to compare the results obtained between the steady and unsteady ground models, the steady conditions will simulate the conditions of the most unfavourable day of the year. Since temperature increase is associated with an acceleration of the various processes that degrade water quality, the worst summer scenario (i.e. maximum temperature gradient during summer) will be analysed here. The parameters that condition the ground behaviour over the year assuming a sand backfill have already been presented (see Table 1 and Figure 2). A wet sand will be assumed in this work to simulate the greatest possible amplitude of the ground temperature over the year and greatest heat transfer from the water, so shortest transition zones. This worst case will be important to test if the steady solution can approximate the unsteady solution in Section 3.2. The maximum daily average of the undisturbed ground temperature at $z_p = 1$ m considering a wet sand is 17.5°C.

The incoming fluid temperature is also a required input. In this work, an annual variation is also assumed for the incoming water. The same amplitude of the ground at $z = 0$ m (i.e. ground surface) is assumed, but the input water temperature is considered to be as lagged as the temperature of the ground at $z_p = 1$ m (considering a wet sand) to account for the time that it takes the water to adapt to atmospheric changes (see Figure 4 later on). In reality, each case will have specific conditions depending on the volume of the service reservoir, its relative position to the ground, etc., but this assumption is reasonable for this case study, where the aim is to assess general trends and behaviours. The maximum daily average of the input water is therefore 20.0°C. These values are consistent with the expected reality in a pipeline system during summer: water is warmer than the ground, so it will cool over the pipeline.

3.1 Steady ground model

This subsection compares the water temperatures computed when assuming a ground finite heat capacity (i.e. coupled model) as opposed to the traditional ground infinite heat capacity hypothesis (i.e. decoupled model). Transition regions are also computed thanks to Eqs. (13a) and (13b) for different materials, diameters and hydraulic conditions. This analysis will answer the first two specific aims of this work. Note that results obtained with the infinite heat capacity hypothesis are equivalent to those computed for DWDS by making use of EPANET-MSX software (or any other 1-D numerical model suited for temperature analysis).

Figure 3 shows the water temperature evolution along the pipe according to Eq. (8). The water temperature has been computed by assuming a finite ground heat capacity model (thermal resistance as in Eq. 9a) and an infinite ground heat capacity model (thermal resistance as in Eq. 9b) for a $r_i = 0.15$ m pipe (300 mm internal diameter) made of CI (CI300), AC/C (AC/C300), PE (PE300) and PVC (PVC300). Figure 3a shows that it takes over 55 km (approximately 31 h) for the water to attain the undisturbed ground temperature according to the finite ground heat capacity (i.e. coupled) model in a CI pipe. This transition length reduces to virtually zero when assuming an infinite ground heat capacity (i.e. decoupled) model. A similar underestimation is observed in Figures 3b, 3c and 3d for the rest of materials. For example, 83 km / 46 h (finite) and 26 km / 14

h (infinite) are needed in the case of a PVC pipe. These results suggest that assuming infinite heat capacity is not an acceptable simplification for appreciable distances/times into the DWDS.

The transition length can be explicitly computed by making use of Eq. (13a) (finite ground heat capacity) or (13b) (infinite ground heat capacity) and a specified tolerance value ($tol = 0.1°C$). Table 3 shows the importance of the terms involved in the computation of the transition length for the four materials under the two hypotheses. This table shows that R_{ground} is greater in order of magnitude than R_{pipe}. This explains the significant differences perceived in Figure 3: a decoupled approach neglects the most important thermal resistance. This table also shows that the water convection term is almost negligible regardless of the material. This means that the transition length depends almost linearly on water velocity (i.e. it is proportional to the flow rate) and quadratically on pipe diameter.

Table 4 shows the computed transition lengths for different pipe materials, diameters and water velocities. Note that some transition lengths exceed the maximum length plotted in Figure 3 (125 km), due to the explicit nature of Eqs. (13a) and (13b). Transition region values for $v = 0.5m/s$ and pipe diameter 300 mm coincide with those in Table 3. Table 4 shows that CI and PVC have extreme behaviours, leading to minimum and maximum transition lengths, respectively, for a given pipe diameter and water velocity. Moreover, it pinpoints that the transition length/residence time increases with pipe diameter, whereas the equivalent residence time is approximately the same no matter the water velocity. A 0.1 m/s water velocity has been adopted to highlight this point. This means that for a specific pipe (installed at a given depth, surrounded by a specific ground, and with a predefined material and pipe diameter), the residence time and the temperature gradient determine the distance required for heat equilibrium to be achieved. Depending on the water velocity, this is associated with a shorter or longer transition distance.

It is important to highlight that the previously computed transition lengths correspond to the steady conditions during the day of summer associated with the maximum gradient. This scenario is associated with maximum differences between the input water and the undisturbed ground temperatures, leading to maximum transition lengths. In spring and autumn, the temperature

gradient between the water and the ground is minimum and influence lengths will reduce (see Eqs. 13). The winter scenario is opposite to the summer day here analysed. Note that the infinite ground heat capacity model underestimates water temperature in summer, which is unfavourable when assessing the impacts of climate change in water quality. Winter would be associated with mirror images for Figures 3a to 3d, i.e. temperature would be overestimated with the infinite heat capacity hypothesis during winter.

3.2 Unsteady ground model

This subsection intends to explore if the steady ground model equations previously applied can be used to approximate the unsteady interaction of the ground over the year (third aim). This implies testing if annual variations are sufficiently slow, so that water temperatures can be approximated with a pseudosteady approach (i.e. steady state every hour) as an alternative to the complex unsteady ground model presented in Section 2.3. Only the finite heat capacity of the ground will be considered for this purpose, because it has already been shown that decoupled models do not sufficiently represent reality for significant distances/times. Simulations are carried out with the original case study (r_i = 0.15 m, L = 125 km, v = 0.5 m/s) and only the two materials identified as extreme in Section 3.1 (CI and PVC) will be here assessed. Regarding spatial discretization, L_i = 500 m (n_s = 250) will be assumed to start with, although its sensitivity will be tested later on.

Figure 4 shows the output water temperature evolution for CI300 and PVC300 pipes at a distance of 25 km from the inlet. This distance has been selected as an arbitrary position within the transition region, so that the difference between materials is noticeable (i.e. temperature equilibrium has not been reached). Figure 4a shows that the water temperature 25 km far from the inlet is close to the ground temperature for CI. This temperature is slightly higher (i.e. closer to the input water temperature) in the PVC pipe (Figure 4b). This result makes intuitive sense due to the higher conductivity of CI, which speeds the heat transfer process and is associated with temperatures closer to the undisturbed ground temperature at the analysed position (i.e. shorter transition length). In both cases, results obtained with the unsteady and pseudosteady approximations are almost identical. They show that, as expected, water heats through the pipeline in winter and cools

along the pipe in summer.

In order to compare the transition regions computed with the unsteady and pseudosteady models, the temperature evolution over the pipe is represented at the worst hour of summer (i.e. the summer day associated with the greatest temperature gradient) in Figure 5a for both CI300 and PVC300 pipes. These figures show that there is a slight difference between the temperature computed with the unsteady and pseudosteady models. This is negligible in comparison with other uncertainties in DWDS modelling and water quality reactions in general (Machell and Boxall 2012). Table 5 shows the transition lengths computed for the CI and PVC pipes with the unsteady (L_i = 500 m) and pseudosteady (Eq. 13a) ground models. Pseudosteady results are equal to those obtained with the steady equation (see Table 4), and they are both longer than those obtained with the unsteady simulation. However, the steady/pseudosteady model provides a reasonable approximation to the unsteady model results. In order to illustrate that this difference is not a consequence of the selected spatial discretization, the unsteady model has also been run with L_i = 250 m. Table 5 shows that transition lengths are still slightly overestimated (<10%) with the steady/pseudosteady approach. Note that implementing the unsteady ground model in an Intel Core i7-6700 CPU 3.40 GHz 32 GB RAM desktop computer (using Matlab R2021a) takes 2018 s (CI300) and 1931 s (PVC300) for L_i = 500 m. These times go up to 7505 s (CI300) and 7332 s (PVC300) when considering L_i = 250 m, whereas the computational cost of the steady/pseudosteady approach is negligible.

Results show that assumed annual changes are sufficiently slow, and the steady/pseudosteady approach can be applied instead of the unsteady ground model to roughly approximate water temperatures and transition lengths. It could be argued that this conclusion is only valid for this particular case study. In order to test its sensitivity, the amplitude of the undisturbed ground and input water temperatures is doubled (A = 20°C). This is an exaggeration of reality (it would lead to ground and water temperature values below 0ºC), but it can be used to check if this simplification works even when seasonal changes are extreme. Figure 5b shows the water temperature evolution along the CI300 and PVC300 pipes. Like before, the distribution obtained with the unsteady (L_i = 500 m) and steady/pseudosteady model is reasonably close, and so are the transition lengths

(see Table 5). Note that this scenario implies doubling the temperature gradient, so the transition length increases less than twice (natural algorithm of the gradient) with respect to the original values.

Temperature analysis is case specific, but adopting a steady/pseudosteady approach to analyse how water temperatures and associated transition lengths vary over the year seems to be a reasonable approximation. These analytical expressions could constitute a useful tool to identify the areas of the network where complex heat transfer phenomena take place.

DISCUSSION

Results show that the effects of water-ground interaction are important many kilometres/hours into a pipeline system. This means that those areas of the network associated with residence times below a threshold value (which depends on pipe characteristics) are subjected to interaction impacting the water temperature. Residence times may vary widely for different network layouts. Machell and Boxall (2014) published a statistical analysis of the water age at two networks. They identify 9.44 h and 19.86 h as the average water age in these systems, but 5.28 h and 2.68 h as the mode of the mean age in these networks. Mode values are near or below the 5-7 h threshold that corresponds to the transition region of CI and PVC (extreme materials) 100 mm pipes according to a coupled model (see Table 4). Note that this threshold would rise if larger diameters were present. This means that a significant number of pipes are likely to be affected by this interaction, so assuming infinite ground capacity may be a poor simplification for significant parts of a DWDS.

The transition region has further implications on water quality analysis. For example, the bulk decay coefficient (k_b), which partly explains chlorine decay at DWDS, varies with temperature according to the Arrhenius formula. Wall reactions are also likely to be temperature dependent, but given the far greater uncertainty of these coefficients, temperature effects remain unknown. Figure 6 shows that a small change in temperature may lead to significant variations in k_b, depending on the activation coefficient (E/R). Chlorine bulk decay behaves exponentially with k_b coefficient, so temperature should be evaluated and conveniently considered when analysing chlorine decay (Díaz and González 2022). There is usually little data available on which to base k_b values,

and there is typically poor control about whether the assumption of constant temperature over the simulation period provides sufficient accuracy for chlorine simulation. This is particularly true as simulation periods increase for more complex networks with longer residence times. Other water quality parameters and processes will also be affected, from corrosion rates to biological growth. Considering planktonic bacteria which are commonly expected to follow exponential growth trends, meaning increasing numbers towards the extremity of networks, these temperature simplifications may not be significant. But if we consider that >95% of organics including bacteria are in biofilms that are fixed to the pipe walls throughout DWDS (Douterelo et al. 2018), these temperature effects will be important. This is amplified when considering that accelerated growth in summer (due to increased temperature - Calero et al. 2021) or die off (due to the reverse) in winter will seed the entire network. The same applies to reaction precipitations (like iron and manganese), which determine discolouration (Mounce et al. 2016). In other words, at the far extremes of networks either modelling approach will predict that water temperature has approximated ground temperature, so which model is used is not significant for temperature driven effects at such locations. What is important is the temperature driven effects over the complete route to such locations, which will determine the quality of water arriving and then changing further at these locations. This modelling study shows that ignoring ground heat capacity effects could be significant for this.

One of the strengths of this work is that it presents an analytical explicit equation to compute the transition length/time. This is possible because the propagation of transport effects (i.e. plug flow along the pipeline) has been disregarded. This means that the thermal balance within the pipe is not considered in the steady equation nor the unsteady model, which accounts for the temporal storage of heat in the ground but not in the water. Assessing the effect of water propagation and analysing the added resolution/need of considering daily patterns or even more random stochastic behaviours (Blokker et al. 2011) is a subject for further research. Addressing this issue is needed to extend the ground finite heat capacity analysis throughout DWDS.

This work shows that ground characteristics and pipe materials determine the size of the transition region. An average wet sand has been considered in this analysis to maximise seasonal

variations, which is important to validate the steady/pseudosteady approach as a reasonable approximation to the unsteady ground model. If pipe backfill was dry (low conductivity), the thermal resistance would increase, and so would the associated transition length/time according to Eq. (13a) (see Figure S1 in supplemental data). Ground moisture content varies in reality depending on weather conditions evolution, ground surface characteristics (e.g. grass vs paved surfaces), street flushing, possible leaks, etc. Similarly, a pipe depth of 1 m (sufficient to assume that the undisturbed ground does not experience daily variations) has been here considered. Results do not vary as much when increasing the installation depth to 2.5 m (see Figure S2 in supplemental data). Pipe characteristics, pipe diameter and conductivity have shown to have a significant effect in the thermal behaviour due to their relative importance in Eqs. (9a) and (13a).

Water temperature behaviour is case specific, and we currently do not really know how much detail/complexity should be included in a model to simulate realistic temperature behaviours, because there has been insufficient data collected. Water temperatures are typically only measured and recorded at the exit of water treatment works and/or (very limited amount of data) at consumer taps (Agudelo-Vera et al. 2020). Limited data makes validation only possible at these points. Hence why prior research in DWDS has not considered the transition zone. While this paper shows mathematically that the transition zone is significant, and this finding is consistent with the modelling approaches typically adopted for sewer systems (finite heat capacity over an influence area) and GSHP (finite heat capacity), no data exists to verify this. Temperature measurements from physical experiments are needed to further understand temperature dynamics and for model validation. These should cover different spatial and temporal scales under realistic conditions, this could be via suitably complex and scale laboratory conditions initially but is likely to require measurements from DWDS operations. Only then will it be possible to assess to what level of complex models are really needed. The data required includes temperature monitoring but also ground surveys and site inspections (e.g., pipe installation details, weather studies). Accurate hydraulic travel times will also be necessary, requiring more than pressure data for headlosses (Boxall et al. 2004). What is clear is that temperature discussions are especially pressing in the

face of climate change. Global warming is expected to increase average temperatures, but also to intensify the frequency of extreme phenomena (e.g. heat waves). Their effect in DWDS water quality should also be assessed (Pick et al. 2021).

CONCLUSIONS

This paper assesses the effect of considering finite ground heat capacity when modelling water temperatures in DWDS. This improvement with respect to the few available previous implementations in water supply systems shows that there is a significant transition region between the temperature at the inlet (conditioned by water treatment works and/or service reservoirs) and that at consumer taps (mostly conditioned by the undisturbed ground temperatures). Results for an average pipe early in the system show that the transition region expands at least 5-6 hours in terms of residence time, meaning that the complex water-ground heat interaction process is of importance for a number of pipes within the DWDS. This shows that the traditional assumption of considering an infinite heat capacity for the ground is not enough over this transition area, providing a poor representation of reality.

An analytical explicit equation is here provided to quantify the transition length/time under steady flow and ground conditions. It shows that, for a pipe with a predefined diameter and material, installed at a specific depth within a conductive ground environment and an input water – undisturbed ground temperature gradient, the transition length is mainly characterized by the residence time, and water velocity determines the distance over which this transition to equilibrium takes place. This expression also seems to be a good first approximation to the results obtained with complex unsteady ground models, which are time-consuming to run. This analysis must be improved to include the thermal balance within the pipeline and so characterise temperature behaviour for unsteady flows, which are out of the scope of this paper.

This work builds on the temperature modelling strategy typically adopted at DWDS. Since temperature drives all reactions and processes from chlorine decay to corrosion and biofilm growth, characterizing this variable is important to ensure the supply of safe clean water at the tap.

DATA AVAILABILITY STATEMENT

Models and code that support the findings of this study are available from the authors upon reasonable request.

ACKNOWLEDGEMENTS

The authors would like to thank the financial support provided by the Spanish Ministry of Science and Innovation - State Research Agency (Grant PID2019-111506RB-I00 funded by MCIN/AEI/10.13039/501100011033) and Junta de Comunidades de Castilla-La Mancha (Grant SBPLY/19/180501/000162 funded by Junta de Comunidades de Castilla-La Mancha and ERDF A way of making Europe). Sarai Díaz would like to thank the financial support provided by the University of Castilla-La Mancha to visit the University of Sheffield in 2021.

REFERENCES

Abdel-Aal, M., Smits, R., Mohamed, M., de Bussem, K., Schellart, A., and Tait, S. (2014). "Modelling the viability of heat recovery from combined sewers." *Water Science and Technology*, 70(2), 297–306.

Agudelo-Vera, C., Avvedimento, S., Boxall, J., Creaco, E., de Kater, H., Di Nardo, A., Djukic, A., Douterelo, I., Fish, K., Iglesias, P., Jacimovic, N., Jacobs, H., Kapelan, Z., Martínez, J., Montoya, C., Piller, O., Quintiliani, C., Rucka, J., Tuhovcak, L., and Blokker, M. (2020). "Drinking water temperature around the globle: Understanding, policies, challenges and opportunities." *Water*, 13, 1049.

Blokker, E., Beverloo, H., Vogelaar, J., Vreeburg, J., and van Dijk, J. (2011). "A bottom-up approach of stochastic demand allocation in a hydraulic network model: a sensitivity study of model parameters." *Journal of Hydroinformatics*, 13(4), 714–728.

Blokker, E. and Pieterse-Quirijns, E. (2013). "Modeling temperature in the drinking water distribution system." *Journal American Water Works Association*, 105(1), E19–28.

Blokker, M., Vreeburg, J., and Speight, V. (2014). "Residual chlorine in the extremities of the drinking water distribution system: the influence of stochastic water demands." *Procedia Engineering*, 70, 172–180.

608 Boxall, J., Saul, A., and Skipworth, P. (2004). "Modelling for hydraulic capacity." *Journal of the*
609 *American Water Works Association*, 96(4), 161–169.
610 Calero, C., Boxall, J., Soria-Carrasco, V., Martínez, S., and Douterelo, I. (2021). "Implications of
611 climate change: How does increased water temperature influence biofilm and water quality of
612 chlorinated drinking water distribution systems?." *Frontiers in Microbiology*, 12, 658927.
613 Canal de Isabel II (2021). "Normas para redes de abastecimiento (in spanish)." *Canal de Isabel II,*
614 *Madrid, Spain*.
615 Claesson, J. and Dunand, A. (1983). *Heat Extraction from the ground by horizontal pipes: A*
616 *mathematical analysis. Report No. D1*. Swedish Council for Building Research, Stockholm,
617 Sweden.
618 Cook, D., Husband, P., and Boxall, J. (2015). "Operational management of trunk main discolour-
619 tion risk." *Urban Water Journal*, 13(4), 382–395.
620 Díaz, S. and González, J. (2022). "The importance of water temperature in water supply systems
621 (in Spanish)." *Ingeniería del Agua*, 26(2), 107–123.
622 Douterelo, I., Calero-Preciado, C., Soria-Carrasco, V., and Boxall, J. (2018). "Whole metagenome
623 sequencing of chlorinated drinking water distribution systems." *Environmental Science: Water*
624 *Research and Technology*, 4, 2080–2091.
625 Durrenmatt, D. and Wanner, O. (2008). "Simulation of the wastewater temperature in sewers with
626 TEMPEST." *Water Science and Technology*, 57(11), 1809–1815.
627 Çengel, Y. and Ghajar, A. (2011). *Heat and Mass Transfer: Fundamentals and Applications, 4th*
628 *edition*. McGraw-Hill, Portland, USA.
629 Eskilson, P. (1987). "Thermal analysis of heat extraction boreholes." Ph.D. thesis, University of
630 Lund, Sweden.
631 Fisher, I., Kastl, G., and Sathasiva, A. (2012). "A suitable model of combined effects of temperature
632 and initial condition on chlorine bulk decay in water distribution systems." *Water Research*, 46,
633 3293–3303.
634 Fontaine, P., Marcotte, D., Pasquier, P., and Thibodeau, D. (2011). "Modeling of horizontal

635 geoexchange systems for building heating and permafrost stabilization." *Geothermics*, 40, 211–
636 220.

637 Gan, G. (2019). "A numerical methodology for comprehensive assessment of the dynamic thermal
638 performance of horizontal ground heat exchangers." *Thermal Science and Engineering Progress*,
639 11, 365–379.

640 Husband, P., Boxall, J., and Saul, A. (2008). "Laboratory studies investigating the processes leading
641 to discolouration in water distribution networks." *Water Research*, 42(16), 4309–4318.

642 Kusuda, T. and Achenbach, P. (1965). "Earth temperature and thermal diffusivity at selected stations
643 in the United States." *National Bureau of Standards, Washington, USA*.

644 Lamarche, L. (2017). "Mixed arrangement of multiple input-output borehole systems." *Applied*
645 *Thermal Engineering*, 124, 466–476.

646 Lamarche, L. (2019). "Horizontal ground heat exchangers modelling." *Applied Thermal Engineer-*
647 *ing*, 155, 534–545.

648 Lamarche, L. and Beauchamp, B. (2007). "A new contribution to the finite line-source model for
649 geothermal boreholes." *Energy and Buildings*, 39(2), 188–198.

650 Machell, J. and Boxall, J. (2012). "Field studies and modeling exploring mean and maximum water
651 age association to water quality in a drinking water distribution network." *Journal of Water*
652 *Resources Planning and Management*, 138(6), 624–638.

653 Machell, J. and Boxall, J. (2014). "Modelling and field work to investigate the relationship between
654 the age and the quality of drinking water at consumer's taps." *Journal of Water Resources*
655 *Planning and Management*, 140(9), 04014020.

656 Marcotte, D. and Pasquier, P. (2008). "Fast fluid and ground temperature computation for geothermal
657 ground-loop heat exchanger systems." *Geothermics*, 37, 651–665.

658 Monteiro, L., Figueiredo, D., Covas, D., and Menaia, J. (2017). "Integrating water temperature in
659 chlorine decay modelling: a case study." *Urban Water Journal*, 14(10), 1097–1101.

660 Mounce, S., Blokker, E., Husband, S., Furnass, W., Schaap, P., and Boxall, J. (2016). "Multivariate
661 data mining for estimating the rate of discolouration material accumulation in drinking water

distribution systems." *Journal of Hydroinformatics*, 18(1), 96–114.

Pick, F., Fish, K., Husband, S., and Boxall, J. (2021). "Non-invasive biofouling monitoring to assess drinking water distribution system performance." *Frontiers in Microbiology*, 12, 730344.

Piller, O. and Tavard, L. (2014). "Modeling the transport of physicochemical parameters for water network security." *Procedia Engineering*, 70, 1344–1352.

Shang, F., Uber, J., and Rossman, L. (2008). "Modeling reaction and transport of multiple species in water distribution systems." *Environmental Science and Technology*, 42(3), 808–814.

Soni, S., Pandey, M., and Bartaria, V. (2015). "Ground coupled heat exchangers: A review and applications." *Renewable and Sustainable Energy Reviews*, 47, 83–92.

Stehfest, H. (1970). "Algorithm 368: Numerical inversion of laplace transform." *Communication of the ACM*, 13(1), 47–49.

van Summeren, J., Raterman, B., Vonk, E., Blokker, M., Van Erp, J., and Vries, D. (2015). "Influence of temperature, network diagonistics and demographic factors on discoloration-related customer reports." *Procedia Engineering*, 119, 416–425.

Villinger, H. (1985). "Solving cylindrical geothermal problems using Gaver-Stehfest inverse laplace transform." *Geophysics*, 50(10), 1581–1587.

WHO (2011). "Guidelines for Drinking-water Quality." *World Health Organization, Geneva, Switzerland*.

Zeng, H., Diao, N., and Fang, Z. (2003). "Heat transfer analysis of boreholes in vertical ground heat exchangers." *International Journal of Heat Mass Transfer*, 46(23), 4467–4481.

List of Tables

TABLE 1. Surface temperature and ground parameters for an average sand: dry sand vs wet sand

	T_0 $(^\circ C)$	A $(^\circ C)$	t_{shift} (h)	k_{ground} $(W/m/K)$	C_{ground} $(J/kg/K)$	ρ_{ground} (kg/m^3)	α_{ground} (m^2/h)
Dry sand	10	10	0	0.95	900	1600	0.0024
Wet sand	10	10	0	3.35	1500	1900	0.0042

TABLE 2. Prototypical pipe material characteristics

	CI	AC/C	PE	PVC
Standard Dimensional Ratio SDR (-)	15	26.5	17	38
Pipe roughness ϵ_{pipe} (mm)	0.2	3	0.03	0.06
Pipe wall conductivity $k_{pipe}(W/m/K)$	60	0.43	0.5	0.16

TABLE 3. Terms involved in the transition region computation (distance and equivalent residence time) for CI300, AC/C300, PE300 and PVC300 under finite and infinite ground heat capacity hypotheses

			R_{ground}	R_{pipe}			
		$Q \cdot \rho_w \cdot C_w$	$\frac{\ln(\frac{2 \cdot z_p}{r_o})}{2 \cdot \pi \cdot k_{ground}}$	$\frac{\ln(\frac{r_o}{r_i})}{2 \cdot \pi \cdot k_{pipe}}$	$\frac{1}{Nu \cdot k_w \cdot \pi}$	$\ln\left(\frac{\lvert T_{in} - T_{ground} \rvert}{tol}\right)$	L_t
		(W/K)	$(m \cdot K/W)$	$(m \cdot K/W)$	$(m \cdot K/W)$	(-)	(km and h)
CI300	Finite	1.4809e5	0.1163	3.7959e-4	5.6611e-4	3.2	56.1 km (31.1 h)
	Infinite		-				0.5 km (0.3 h)
AC/C300	Finite		0.1193	0.0290	3.7088e-4		71.1 km (39.5 h)
	Infinite		-				14.1 km (7.8 h)
PE300	Finite		0.1171	0.0398	6.3262e-4		75.4 km (41.9 h)
	Infinite		-				19.4 km (10.8 h)
PVC300	Finite		0.1205	0.0538	6.1681e-4		83.6 km (46.5 h)
	Infinite		-				26.0 km (14.5 h)

TABLE 4. Transition region (distance and equivalent residence time) for different pipe materials, diameters and water velocities

		CI		AC/C		PE		PVC	
Velocity (m/s)	Diameter (mm)	Finite	Infinite	Finite	Infinite	Finite	Infinite	Finite	Infinite
0.1	100	1.9 km (5.2 h)	0.1 km (0.2 h)	2.2 km (6.1 h)	0.4 km (1.0 h)	2.3 km (6.4 h)	0.5 km (1.4 h)	2.5 km (6.9 h)	0.6 km (1.8 h)
	300	11.4 km (31.7 h)	0.3 km (0.8 h)	14.4 km (39.9 h)	3.0 km (8.2 h)	15.3 km (42.4 h)	4.1 km (11.3 h)	16.9 km (47.0 h)	5.4 km (15.0 h)
	600	32.6 km (90.4 h)	0.7 km (1.9 h)	44.6 km (123.8 h)	11.5 km (32.0 h)	48.0 km (133.3 h)	15.8 km (43.9 h)	54.6 km (151.7 h)	21.1 km (58.7 h)
0.5	100	9.0 km (5.0 h)	0.1 km (0.1 h)	10.7 km (5.9 h)	1.6 km (0.9 h)	11.2 km (6.2 h)	2.2 km (1.2 h)	12.1 km (6.7 h)	2.9 km (1.6 h)
	300	56.1 km (31.1 h)	0.5 km (0.3 h)	71.1 km (39.5 h)	14.1 km (7.8 h)	75.4 km (41.9 h)	19.4 km (10.8 h)	83.6 km (46.5 h)	26.0 km (14.5 h)
	600	160.7 km (89.3 h)	1.3 km (0.7 h)	221.2 km (122.9 h)	56.0 km (31.1 h)	237.9 km (132.2 h)	76.9 km (42.7 h)	271.0 km (150.6 h)	103.5 km (57.5 h)

TABLE 5. Transition region (distance and equivalent residence time) at the worst case summer day according to different finite heat capacity ground models: original vs double temperature amplitude

Temperature amplitude	Ground model	CI300	PVC300
Original (A = 10°C)	Unsteady (L_i = 500 m)	53.5 km (29.7 h)	81.0 km (45.0 h)
	Unsteady (L_i = 250 m)	53.00 km (29.4 h)	80.75 km (44.9 h)
	Pseudosteady (Eq. 13a)	56.1 km (31.1 h)	83.6 km (46.5 h)
Double (A = 20°C)	Unsteady (L_i = 500 m)	65.0 km (36.1 h)	98.0 km (54.4 h)
	Unsteady (L_i = 250 m)	64.25 km (35.7 h)	97.75 km (54.3 h)
	Pseudosteady (Eq. 13a)	68.1 km (37.8 h)	101.6 km (56.4 h)

List of Figures

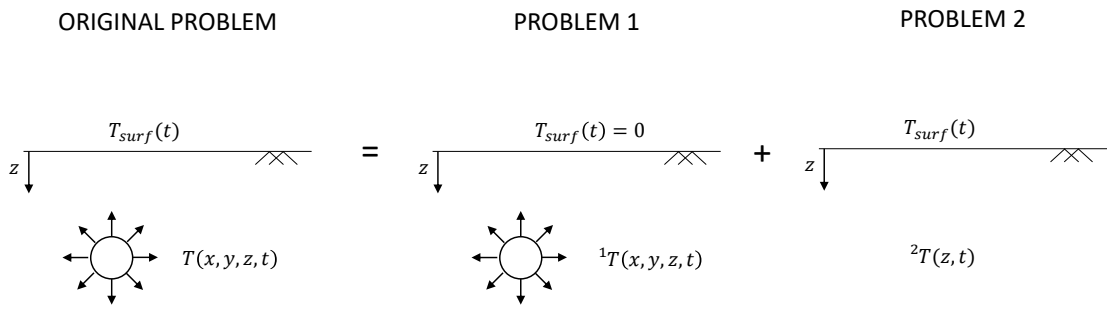

Fig. 1. Superposition principle for heat transfer analysis in a buried pipe

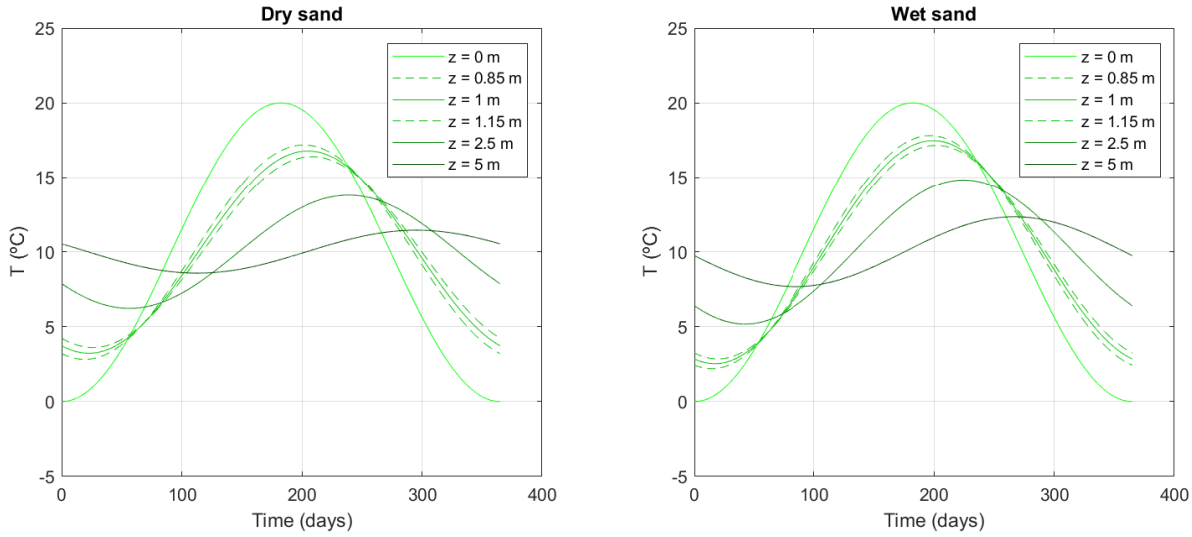

Fig. 2. Undisturbed ground temperature evolution at different depths for an average sand: a) dry sand and b) wet sand

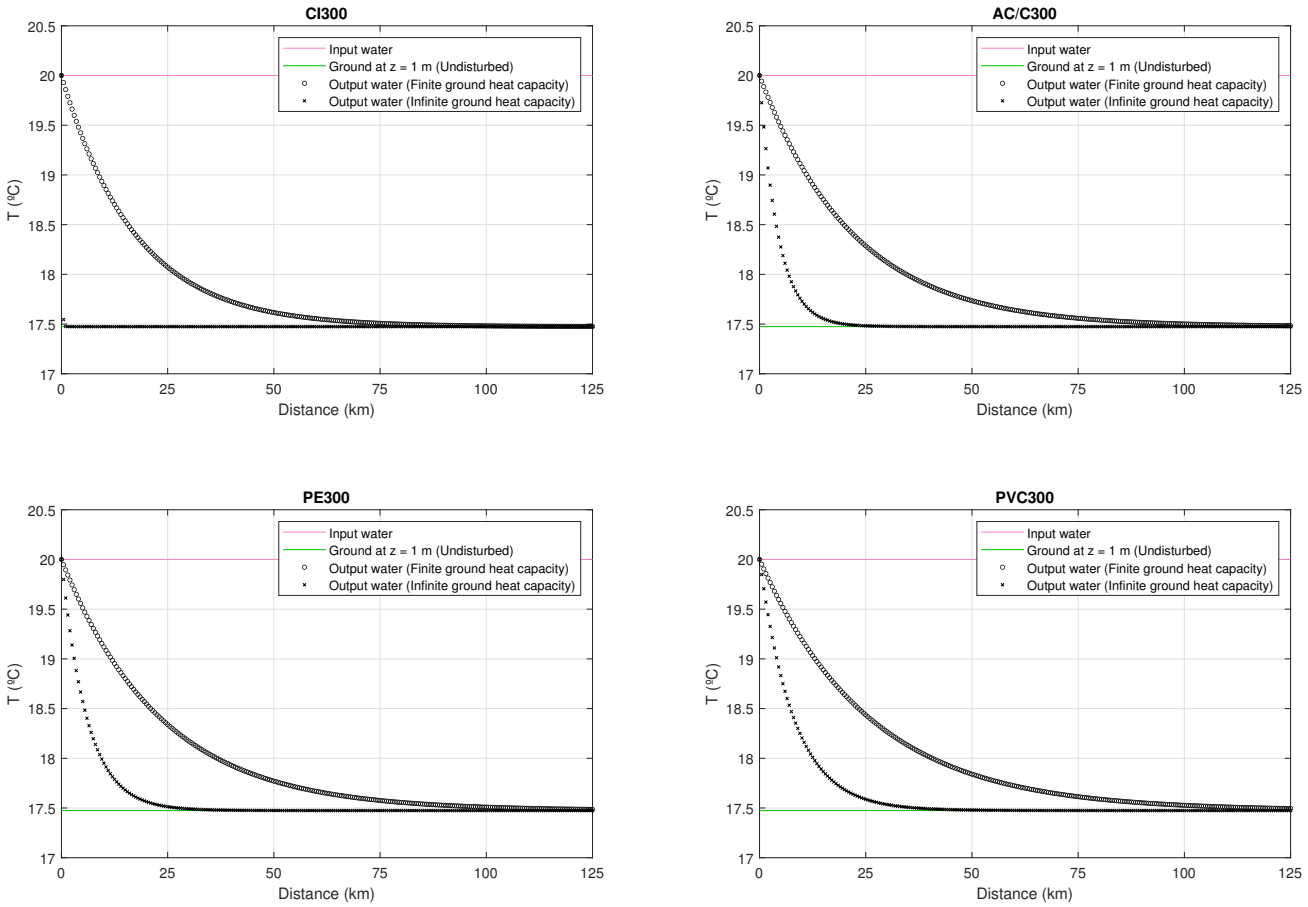

Fig. 3. Temperature evolution along the pipe under steady ground conditions (input water 20.0ºC, ground 17.5ºC) for wet sand and z_p = 1 m: a) CI300, b) AC/C300, c) PE300 and d) PVC300

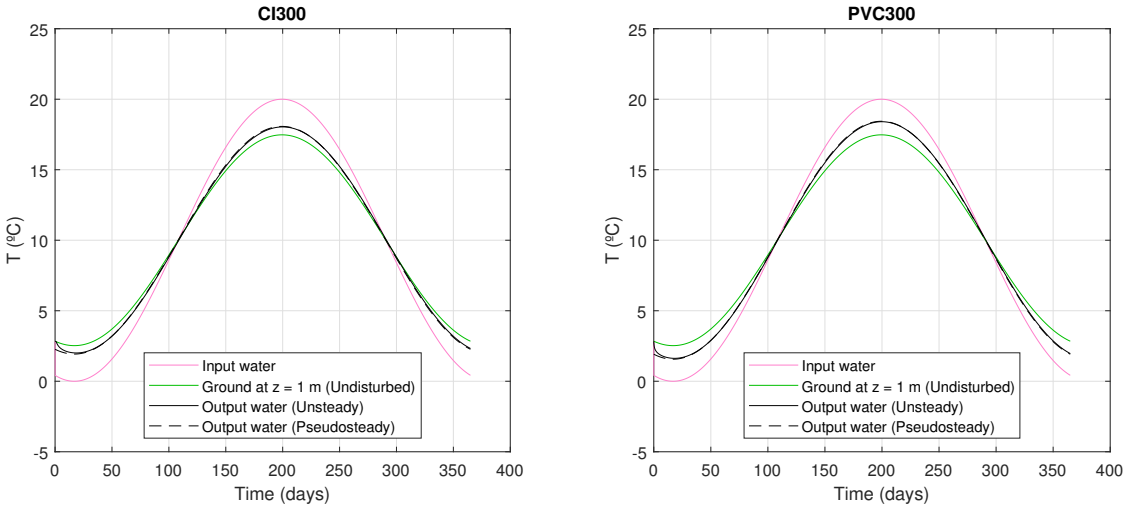

Fig. 4. Annual output water temperature evolution 25 km far from the pipe inlet: a) CI300 and b) PVC300

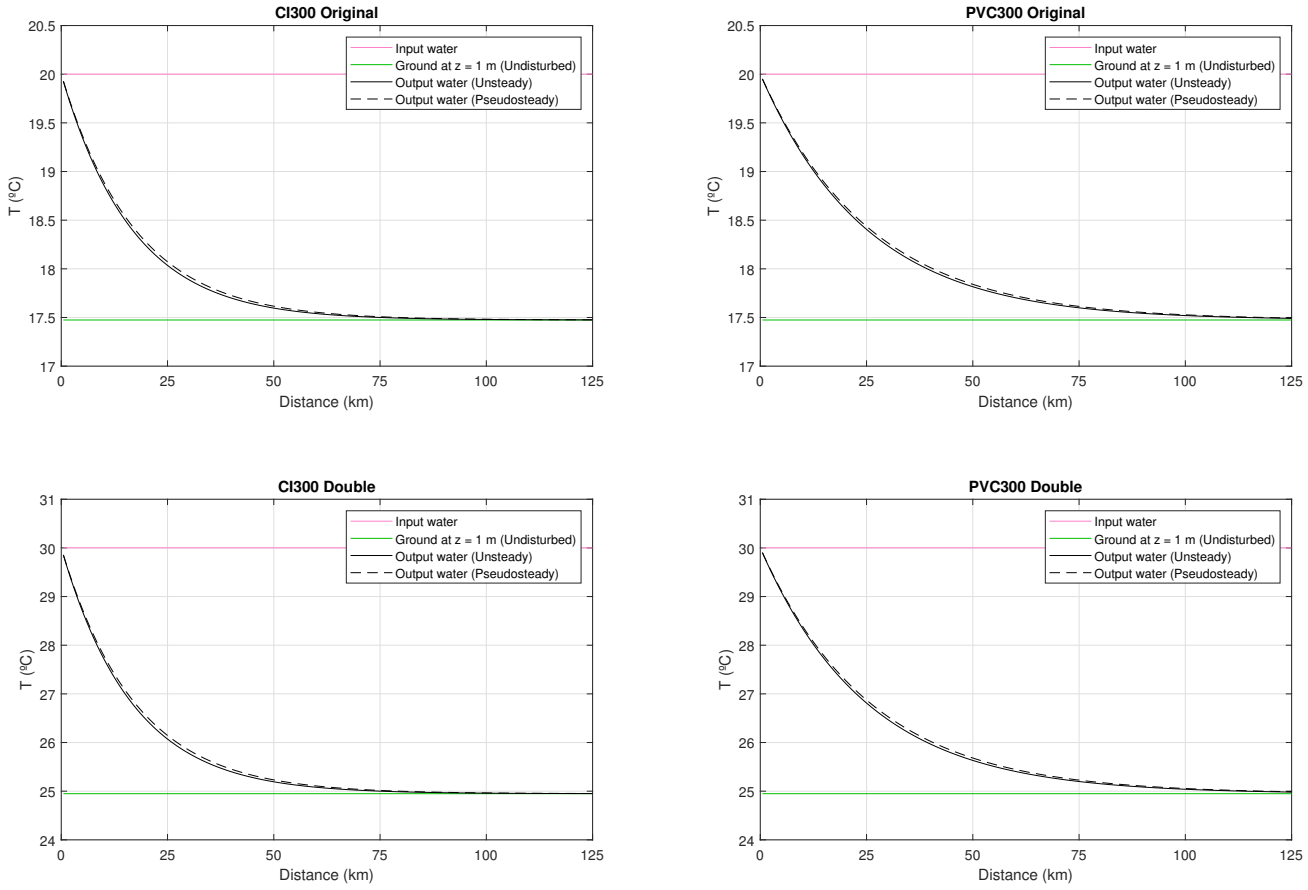

Fig. 5. Temperature evolution along the CI300 and PVC300 pipes under unsteady ground conditions (input water 20.0ºC, ground 17.5ºC): a) original temperature amplitude and b) double temperature amplitude. Note that the y axis range doubles for b)

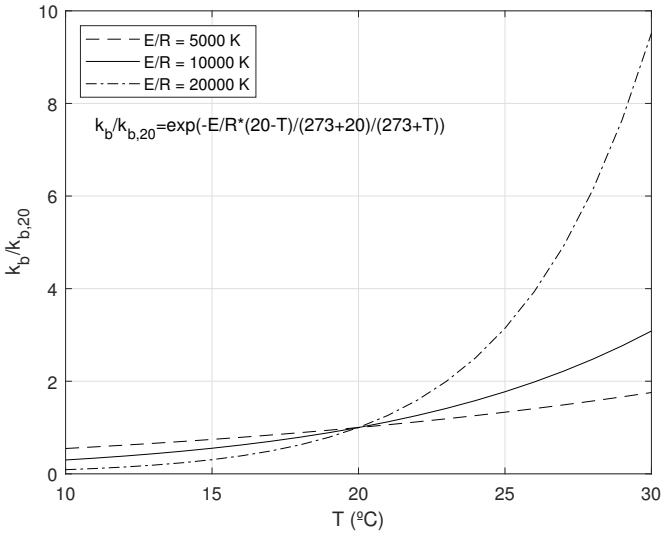

Fig. 6. Chlorine bulk decay coefficient variation with temperature